AUTOIMMUNITY

Antigen-specific depletion of CD4$^+$ T cells by CAR T cells reveals distinct roles of higher- and lower-affinity TCRs during autoimmunity

Jaeu Yi[1]†, Aidan T. Miller[1]†, Angela S. Archambault[2], Andrew J. Jones[1], Tara R. Bradstreet[3], Sravanthi Bandla[2], Yu-Sung Hsu[4], Brian T. Edelson[3], You W. Zhou[5], Daved H. Fremont[3], Takeshi Egawa[3], Nathan Singh[4], Gregory F. Wu[2,3]*, Chyi-Song Hsieh[1]*‡

Both higher- and lower-affinity self-reactive CD4$^+$ T cells are expanded in autoimmunity; however, their individual contribution to disease remains unclear. We addressed this question using peptide-MHCII chimeric antigen receptor (pMHCII-CAR) T cells to specifically deplete peptide-reactive T cells in mice. Integration of improvements in CAR engineering with TCR repertoire analysis was critical for interrogating in vivo the role of TCR affinity in autoimmunity. Our original MOG$_{35–55}$ pMHCII-CAR, which targeted only higher-affinity TCRs, could prevent the induction of experimental autoimmune encephalomyelitis (EAE). However, pMHCII-CAR enhancements to pMHCII stability, as well as increased survivability via overexpression of a dominant-negative Fas, were required to target lower-affinity MOG-specific T cells and reverse ongoing clinical EAE. Thus, these data suggest a model in which higher-affinity autoreactive T cells are required to provide the "activation energy" for initiating neuroinflammatory injury, but lower-affinity cells are sufficient to maintain ongoing disease.

INTRODUCTION

Autoimmunity is thought to arise from self-antigen–reactive effector T cells possibly induced by impaired regulatory T cell (T_{reg}) function or cross-reactivity to foreign antigens. For example, multiple sclerosis (MS) is widely believed to be caused by myelin-specific autoreactive CD4$^+$ T cells (*1*–*3*). Similarly, experimental autoimmune encephalomyelitis (EAE), a murine model of MS, can be driven by self-reactivity to myelin oligodendrocyte glycoprotein (MOG). Classically, immunity is thought to be driven by clonal expansion toward higher-affinity T cell clones (*4*, *5*). Initially, this was also thought to be true for EAE due to the marked expansion of MOG-specific T cells identified using major histocompatibility complex class II (MHCII) tetramers (*6*, *7*). However, it became clear that MHCII tetramers were not identifying the entire population of self-reactive T cells, as revealed by the development of new techniques capable of identifying lower-affinity T cells such as micropipette-based adhesion two-dimensional (2D) affinity assays (*8*, *9*). These data showed that lower-affinity, rather than higher-affinity, MOG-specific CD4$^+$ T cells dominate during EAE (*8*), raising the question of how self-reactive T cells with higher or lower affinity contribute to autoimmunity.

We addressed this question using peptide-MHCII chimeric antigen receptor (pMHCII-CAR) T cells to delete antigen-specific T cells in vivo for the treatment of autoimmunity. We modeled our pMHCII-CAR after the MHCI-specific signaling and antigen-presenting bifunctional receptor (SABR) construct used to assess T cell specificity in vitro (*10*). Our intial MOG pMHCII-CAR construct expressed on CD8$^+$ T cells could efficiently deplete higher-affinity peptide-specific CD4$^+$ T cells in vivo and block initiation of EAE but could not deplete lower-affinity 2D2 T cell receptor (TCR) transgenic (Tg) T cells nor reduce clinical deficits once disease was initiated. Improvements in the pMHCII-CAR construct resulted in higher sensitivity for deletion of 2D2 as well as other lower-affinity autoreactive T cells and ameliorated ongoing clinical disease in EAE. Therefore, these data suggest that higher-affinity autoreactive T cells are criticial for initiation of neuroinflammation, whereas lower-affinity T cells are sufficient to maintain ongoing disease.

RESULTS

Generation of pMHCII-CAR constructs

To develop a CAR that would recognize antigen-specific MHCII-restricted CD4$^+$ T cells, we started with intact MHCII αβ dimers rather than a single chain construct (*11*), reasoning that this may simplify application to other MHCII alleles. We first determined that fusion of a CD28-CD3zeta (28z) signaling domain after the C terminus and not transmembrane (TM) domain of the MHCII I-A^b β chain resulted in the most nuclear factor of activated T cell–green fluorescent protein (NFAT-GFP) signal in T cell hybridoma cells (*12*) upon stimulation with plate-bound anti-MHCII (fig. S1A). Encoding of a peptide in I-A^b β with a 16–amino acid flexible linker (Fig. 1A) (*13*) markedly enhanced the cell surface expression of MHCII (fig. S1B). We then assessed whether the pMHCII-CAR could be triggered by its cognate TCR. Consistent with the results using SABR (*10*), we observed robust activation of ovalbumin (OVA)$_{323–339}$, human class II–associated invariant chain peptide (hCLIP), and lymphocytic choriomeningitis virus (LCMV) glycoprotein (GP)$_{61–80}$ pMHCII-CAR–expressing hybridomas by their

[1]Department of Internal Medicine, Division of Rheumatology, Washington University School of Medicine, St. Louis, MO 63110, USA. [2]Department of Neurology, Washington University in St. Louis, St. Louis, MO 63110, USA. [3]Department of Pathology and Immunology, Washington University School of Medicine, St. Louis, MO 63110, USA. [4]Division of Oncology, Section of Stem Cell Biology, Washington University School of Medicine, St. Louis, MO 63105, USA. [5]Wugen Inc., 4340 Duncan Ave, St. Louis, MO 63110, USA.
*Corresponding author. Email: chsieh@wustl.edu (C.-S.H.); gfwu@wustl.edu (G.F.W.)
†These authors contributed equally to this work.
‡Lead contact.

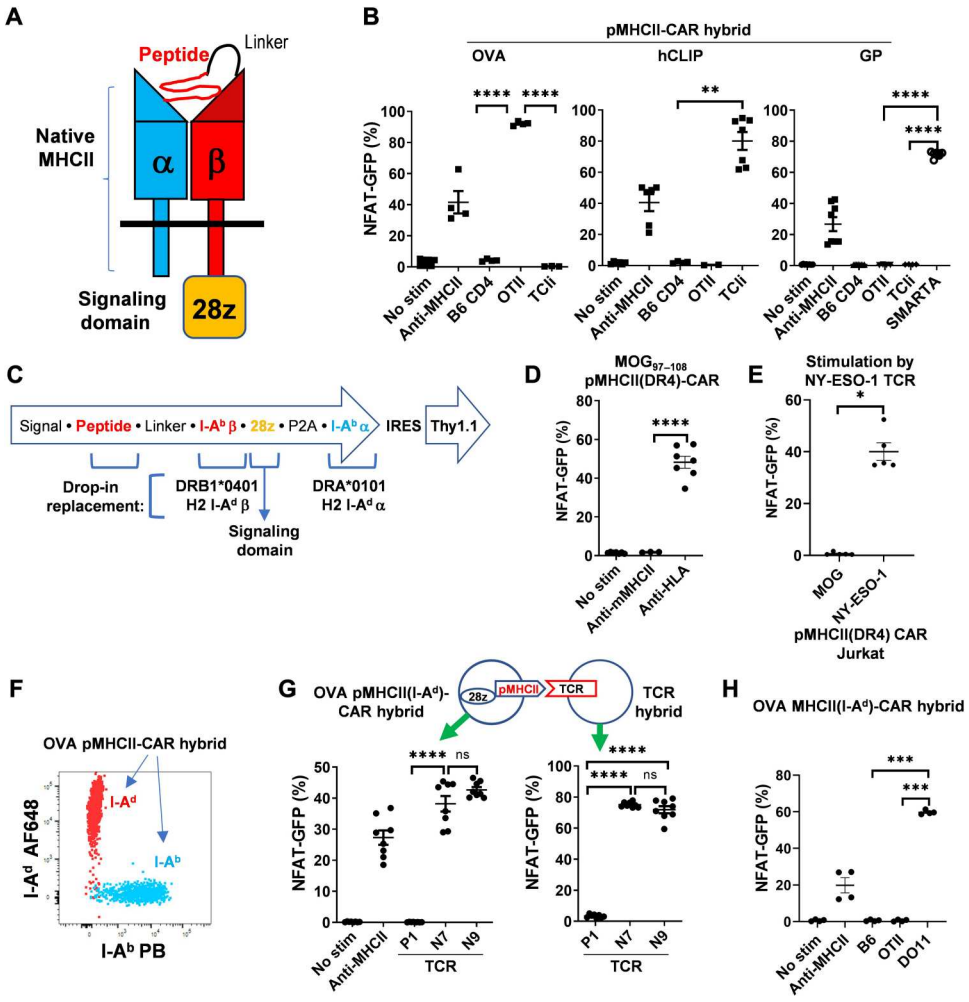

Fig. 1. TCR-specific recognition by pMHCII-CAR. (**A**) Schematic of pMHCII-CAR using intact MHCII molecules. The peptide is attached to I-A^b β via a flexible linker. The signaling domain (28z) is attached to the C terminus of I-A^b β. (**B**) pMHCII-CARs are TCR specific. NFAT-GFP hybridoma cells were retrovirally transduced with the indicated pMHCII-CAR vectors and cocultured with the indicated T cells (expt. = 2 or 3; two or three technical replicates each). NFAT-GFP expression was assessed 2 days later by flow cytometry. Plate-bound anti-MHCII antibody was used as a positive control. (**C**) Diagram of RV construct and feasibility of drop-in replacement of peptide, MHCII, and signaling domain. The MHCIIβ and MHCIIα chains are coexpressed via a (GSG)P2A linker. The reporter Thy1.1 or mCherry is expressed after an IRES. (**D** and **E**) Analysis of an HLA-DR4 pMHCII-CAR. (D) NFAT-GFP signaling of $MOG_{97–108}$ pMHCII(DR4)-CAR–transduced hybridoma cells in response to plate-bound anti–HLA-DR antibody was assessed by flow cytometry 2 days later (expt. = 2; three or four technical replicates each). Anti-mouse MHCII was tested in one experiment. (E) NFAT-GFP signaling of NY-$ESO\text{-}1_{119–133}$ or $MOG_{97–108}$ pMHCII(DR4)-CAR–transduced Jurkat cells was assessed 18 hours after coculture with NY-ESO-1 TCR-expressing Jurkat cells. (**F** and **G**) Analysis of an I-A^d pMHCII-CAR. (F) The FACS plot shows overlaid I-A^d and I-A^b expression of hybridoma cell lines transduced with $OVA_{323–339}$ in either I-A^d or I-A^b pMHCII-CAR constructs. (G) TCR-specific activation of OVA pMHCII(I-A^d)-CAR. Shown are the percentages of NFAT-GFP$^+$ cells among $OVA_{323–339}$ pMHCII(I-A^d)-CAR–expressing (left) or I-A^d–restricted $OVA_{323–339}$–reactive TCR-expressing (right) hybridoma cells that were cocultured for 2 days. I-A^d–restricted $OVA_{323–339}$–reactive clones P1, N7, and N9 were previously described (*16*). (**H**) MHCII-restricted activation of pMHCII-CAR. NFAT-GFP signals induced by B6 or the indicated TCR Tg cells are shown (expt. = 2; two technical replicates each). Bars show means ± SEM. Nested one-way ANOVA with Holm-Sidak multiple comparison test or nested Student's *t* test; ns, not significant; * $P < 0.05$; ** $P < 0.01$; *** $P < 0.001$; **** $P < 0.0001$.

cognate TCRs expressed on OTII, TCli, and SMARTA Tg cells, respectively, but not other TCR specificities or polyclonal CD4$^+$ T cells (Fig. 1B). We continued to use the 28z signaling domain, because it generated a stronger NFAT signal than z alone in hybridoma cells (fig. S1C).

To assess the feasibility of using other MHCII alleles required for personalization of pMHCII-CAR T cell treatment, we tested whether the MHCII α and β chains from other alleles could be directly swapped into the I-A^b construct (Fig. 1C). First, we generated a $MOG_{97–108}$ peptide human leukocyte antigen (HLA)–CAR using the human HLA-DR4 allele with easily detectable cell surface expression and anti–HLA-induced signaling (Fig. 1D and fig. S2A). Consistent with the TCR specificity seen with murine pMHCII-CARs (Fig. 1B), New York esophageal squamous cell carcinoma 1 (NY-ESO-1), but not MOG, pMHCII(DR4)-CAR–expressing Jurkat cells (*14*) were stimulated by NY-ESO-1 TCR-expressing (*15*) Jurkat cells (Fig. 1E). Second, we tested a different murine MHCII, I-A^d. Allele-specific antibodies discriminated between the $OVA_{323–339}$ I-A^d and I-A^b pMHCII-CAR constructs (Fig. 1F). Moreover, $OVA_{323–339}$ pMHCII(I-A^d)-CAR could be activated in

vitro by OVA-specific I-A^d–restricted TCRs (*16*) expressed on hybridoma cells (Fig. 1G). This I-A^d pMHCII-CAR recognized only OVA-specific I-A^d–restricted DO11, but not I-A^b–restricted OTII, T cells (Fig. 1H and fig. S2B). In summary, we generated pMHCII-CAR vectors from three different MHCII alleles, either mouse or human, by simply including different MHCII α and β chains as drop-in replacements, suggesting that this straightforward pMHCII-CAR design is easily adaptable to different MHCII alleles.

TCR-specific CD4$^+$ T cell killing by pMHCII-CAR T cells

A bidirectional assessment of cognate interactions using NFAT-GFP in hybridoma cells suggested that pMHCII-CAR signaling was less efficient than TCR signaling (Fig. 1G) but in the range of TCR interactions with pMHCII presented on dendritic cells (DCs) in our previous studies (*12*, *17*, *18*). We asked whether pMHCII-CARs could be used to target and kill antigen-specific CD4$^+$ T cells in vivo. To test this, we retrovirally transduced pMHCII-CARs into naïve CD8$^+$ T cells activated by anti-CD3 and anti-CD28. Transduction efficiency was routinely more than 40% based on the Thy1.1 reporter (fig. S3A). Surface expression of pMHCII was dependent on the peptide but could be robust (fig. S3). Transfer of pMHCII-CAR–expressing CD8$^+$ T cells into host mice resulted in deletion of only the cognate TCR Tg cells (Fig. 2, A to C), recapitulating the in vitro specificity in vivo. The mesenteric lymph node (MLN) was typically analyzed for in vivo TCR Tg depletion assays, because deletion was equivalent in the MLN and spleen (Fig. 2C), and the MLN exhibited less nonspecific staining than the spleen. Note that CAR T cell transfer was performed into hosts without preconditioning such as lymphodepletion or irradiation. We also tested whether pMHCII-CAR T cells could eliminate activated effector CD4$^+$ T cells, which would be important for the treatment of ongoing immune-mediated disease. CD4$^+$ T cell killing was very efficient, with injection of 22,000 pMHCII-CAR T cells sufficient to eliminate almost all OTII T cells activated by immunization with OVA/IFA (incomplete freund's adjuvant) (Fig. 2, D and E). In summary, these data show that both naïve and activated CD4$^+$ T cells can be efficiently eliminated in vivo using pMHCII-CAR cells in a TCR-specific manner.

Prevention and treatment of central nervous system autoimmunity using pMHCII-CAR T cells

One of the goals for pMHCII-CAR T cell therapy is the treatment of autoimmune disease. However, pathogenic autoreactive TCRs, in comparison with the foreign reactive TCRs studied above, may be of lower affinity due to encounter of antigen in the thymus, resulting in negative or T_{reg} selection (*16*, *19*, *20*). To test the impact of lower-affinity pMHCII-TCR interactions, we used a previously described altered peptide ligand of OVA peptide, OVA_{E336Q}, which shows decreased stimulation of OTII T cells compared with wild-type (WT) OVA (*21*, *22*). We found that OVA_{E336Q} pMHCII-CAR was less efficient at in vitro activation or in vivo deletion compared with WT OVA (Fig. 3, A and B) with similar surface expression (fig. S3B). The lower-affinity OVA_{E336Q}, but not WT $OVA_{323–339}$, pMHCII-CAR was dependent on CD4 for in vitro signaling (Fig. 3B), suggesting that the use of an intact MHCII molecule can facilitate CAR signaling by co-receptor engagement. This does not appear to be possible with the previously reported pMHCII-TCR fusion due to the lack of a CD4 binding site (*23*). In summary, these data suggest that pMHCII-TCR affinity dictates the efficiency of target cell recognition and killing by pMHCII-CAR T cells.

We then asked whether $MOG_{35–55}$ pMHCII-CAR would recognize 2D2 TCR Tg cells (*24*), which can be used to induce EAE but have been reported to have low affinity for $MOG_{35–55}$ (*9*, *25*). However, 2D2 T cells did not activate pMHCII-CAR–expressing NFAT-GFP reporter hybridoma cells (Fig. 3C), which may be partially explained by the low surface expression of the $MOG_{35–55}$ pMHCII-CAR compared with OVA or GP peptide constructs (Fig. 3D). Consistent with these in vitro results, we did not find evidence of pMHCII-CAR–mediated depletion of 2D2 in vivo (Fig. 3E). Thus, these data predicted that $MOG_{35–55}$ pMHCII-CAR, at least in this original form, would be ineffective against autoimmunity caused by low-affinity self-reactive T cells such as 2D2.

Because 2D2 may not be representative of all encephalitogenic CD4$^+$ T cells, we proceeded to test whether $MOG_{35–55}$ pMHCII-CAR T cells could be used to treat EAE. B6 mice were immunized subcutaneously with $MOG_{35–55}$ peptide in Freund's complete adjuvant (FCA), followed by pertussis toxin (PTX) injection at immunization and 48 hours later. Unexpectedly, injection of $MOG_{35–55}$ pMHCII-CAR T cells at the time of disease onset markedly limited disease activity (Fig. 3F). This corresponded with a decrease in $MOG_{38–49}$ tetramer$^+$ cells in the central nervous system (CNS) (Fig. 3G). Because 2D2 T cells could not be targeted by this pMHCII-CAR (Fig. 3, C and E), our interpretation is that the encephalitogenic T cells inducing active EAE are likely to recognize $MOG_{35–55}$ with a higher affinity than 2D2 T cells.

Disulfide trap enhances pMHCII-CAR expression and sensitivity to low-affinity MOG-specific T cells

To optimize pMHCII-CAR T cell therapy for EAE, our initial goal was to improve the efficiency of deleting low-affinity T cells, given our inability to target 2D2 T cells. Because the cell surface expression of $MOG_{35–55}$ pMHCII-CAR was low (Fig. 4A), we tested modifications that could improve pMHCII stability. We used an artificial "disulfide trap" (DST) that cross-links a cysteine in the linker (p9 + 2 position) attached to I-A^b β with a mutated cysteine at I-A^b α72 to stabilize the pMHCII molecule (*26*). Consistent with reports showing improved pMHCII stability in MOG tetramers (*26*), we also observed markedly improved surface expression of MOG_{DST} pMHCII-CAR (Fig. 4A). MOG_{DST} pMHCII-CAR facilitated NFAT-GFP induction in vitro in response to 2D2 when expressed in hybridoma cells (Fig. 4B) and depletion of 2D2 cells in vivo when expressed in CD8$^+$ T cells (Fig. 4C). Despite the improvements afforded by MOG_{DST} in terms of pMHCII expression and 2D2 recognition and killing, MOG_{DST} pMHCII-CAR T cells did not statistically improve upon $MOG_{35–55}$ pMHCII-CAR T cell therapy of EAE (Fig. 4D). These results suggest that, although MOG_{DST} pMHCII-CAR T cells may be able to recognize and deplete a wider affinity range of MOG-reactive T cells, additional modifications are necessary to enhance their efficacy for the treatment of EAE.

Inhibition of Fas enhances pMHCII-CAR T cell survival and lethality

A potential avenue for enhancing CAR T cell efficacy was suggested by the in vivo 2D2 deletion experiment, where we noted a low rate of MOG_{DST} pMHCII-CAR T cell survival (Fig. 4C). We therefore tested modifications reported to enhance CAR T cell survival,

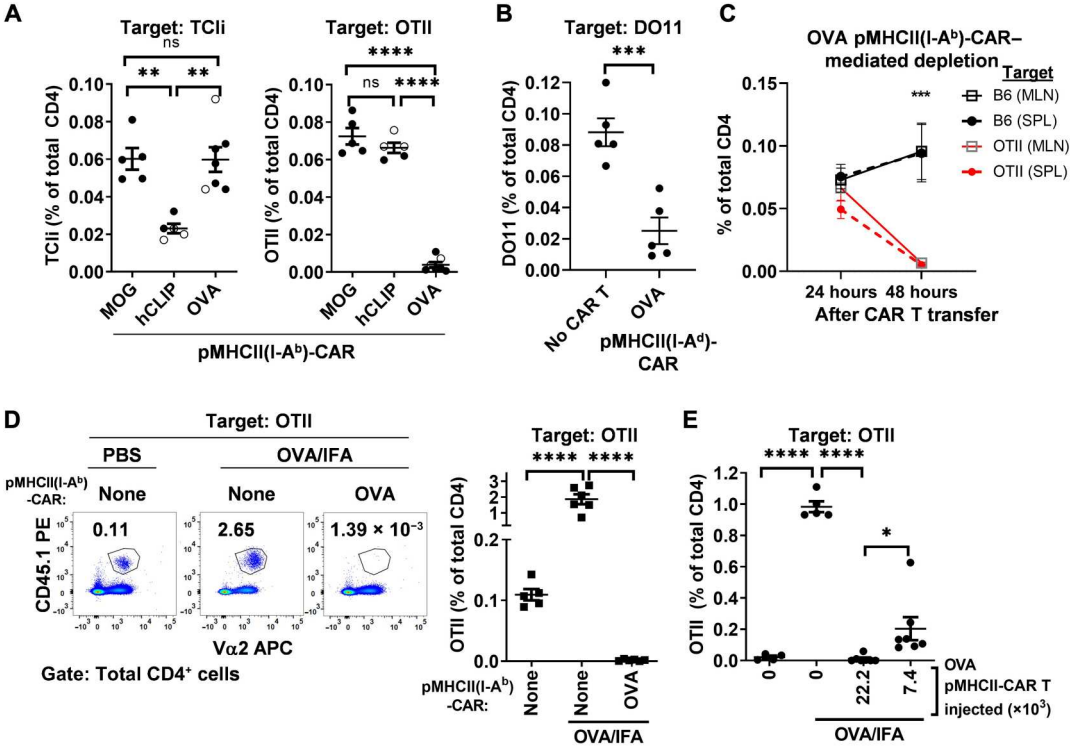

Fig. 2. Killing of cognate CD4⁺ T cells by pMHCII-CAR T cells in vivo. (**A** and **B**) TCR-specific depletion of naïve CD4⁺ T cells by pMHCII-CAR T cells. Sorted naïve ($CD44^{lo}$ $CD62L^{hi}$) $CD8^+$ T cells were activated in vitro and retrovirally transduced with the indicated pMHCII-CAR vectors. (A) A total of 2×10^5 OTII and TCIiαβ TCR Tg T cells were injected intravenously into B6 mice 1 day before transfer of 2×10^5 CAR T cells. MLNs were harvested after 7 days, and target cell deletion was analyzed by flow cytometry. OTII and TCIiαβ cells were identified by Vα2 and Vβ6 expressions, respectively, among total donor CD45.1 CD4⁺ T cells. Percentages of TCIiαβ (left) or OTII (right) cells of the total CD4⁺ T cells under each condition are shown (expt. = 2; $n = 5$ to 7 per group). Open and closed symbols indicate hosts with TCR Tg cells injected individually versus together, respectively. (B) $OVA_{323–339}$ pMHCII(I-A^d)-CAR–expressing BALB/c $CD8^+$ T cells (1×10^6) were used to target DO11 T cells (2×10^5) transferred 1 day prior. Anti-clonotype antibody (KJ1-26) was used to identify the percentage of DO11 cells of total CD4⁺ T cells at harvest (expt. = 2; $n = 5$ per group). (**C**) Rapid depletion of OTII cells by pMHCII-CAR T cells in the MLN and spleen. Congenically marked OTII and B6 naïve CD4⁺ T cells (2×10^5 each) were coinjected 1 day before intravenous transfer of 2×10^5 $OVA_{323–339}$ pMHCII-CAR T cells. The percentages of donor OTII T cells (red) or B6 CD4⁺ T cells (black) among total CD4⁺ T cells in the MLN or spleen are shown at the indicated times after CAR T cell transfer (expt. = 2; $n = 6$ per group). (**D** and **E**) Depletion of activated OTII cells by $OVA_{323–339}$ pMHCII-CAR T cells. Host B6 mice were injected with 2×10^5 OTII cells and immunized the next day with OVA/IFA, followed 2 days later by pMHCII-CAR T cells injection [2×10^5 in (D) or as indicated in (E)]. OTII cell depletion was examined 5 days later [expt. = 2; $n = 5$ or 6 (D) or $n = 4$ to 7 (E) per group]. *P* values were determined by one-way ANOVA with Holm-Sidak, except (B) Student's *t* test and (C) repeated-measures ANOVA. Bars show means ± SEM; $^*P < 0.05$; $^{**}P < 0.01$; $^{***}P < 0.001$; $^{****}P < 0.0001$.

including overexpression of B cell lymphoma 2 (Bcl2) (*27*) and inhibition of Fas signaling via overexpression of a dominant-negative Fas with a deleted death domain ($Fas^{\Delta DD}$) (*28*). These genes were incorporated into the 3′ end of the vector using a T2A sequence. In comparison with MOG_{DST} alone, the overexpression of $Fas^{\Delta DD}$ but not Bcl2 markedly increased target 2D2 killing and CAR T cell recovery 5 days after transfer (Fig. 5, A and B, and fig. S4, A and B). However, $Fas^{\Delta DD}$ expression did not facilitate in vivo depletion of 2D2 by T cells expressing the original $MOG_{35–55}$ CAR construct (fig. S4C), suggesting that $Fas^{\Delta DD}$ did not markedly enhance target cell recognition. Rather, $Fas^{\Delta DD}$ may act to block the effect of increased Fas levels seen on MOG_{DST} versus $MOG_{35–55}$ CAR T cells after in vivo interaction with 2D2 cells (fig. S4D) and thereby limit Fas-mediated apoptosis of CAR T cells.

The increased lethality of MOG_{DST} pMHCII-CAR-$Fas^{\Delta DD}$ T cells may simply be due to inhibition of Fas-FasL–mediated cell death of the CAR T cell, resulting in persistent availability to reengage other targets. However, inhibition of Fas may also permit prolonged or higher expression of FasL on the CAR T cell, facilitating killing. We therefore addressed the killing mechanism of pMHCII-CAR T cells using $FasL^{gld}$ mice (*29*), which encode a hypomorph mutation of FasL that markedly reduces Fas-mediated killing (*30*). We found that MOG_{DST} pMHCII-CAR-$Fas^{\Delta DD}$ $CD8^+$ T cells expressing $FasL^{gld}$ show a ~15% reduction in their ability to kill 2D2, whereas perforin deficiency did not affect CAR T cell killing (Fig. 5, C and D).

We then tested the efficacy of MOG_{DST} pMHCII-CAR-$Fas^{\Delta DD}$ in EAE when transferred into mice 12 days after MOG immunization, at which time, on average, half of the mice show initial clinical signs of inflammatory demyelination. Consistent with prior experiments (Figs. 3F and 4D), $MOG_{35–55}$ pMHCII-CAR treatment of mice without signs of EAE was effective at limiting disease, whereas treatment with MOG_{DST} pMHCII-CAR-$Fas^{\Delta DD}$ prevented almost all clinical signs of EAE (Fig. 5E). However, a clear benefit of MOG_{DST} pMHCII-CAR-$Fas^{\Delta DD}$ was observed in mice that had already manifested signs of EAE, with a significant reduction in subsequent clinical scores, whereas initially symptomatic $MOG_{35–55}$ pMHCII-CAR–treated mice remained clinically unchanged

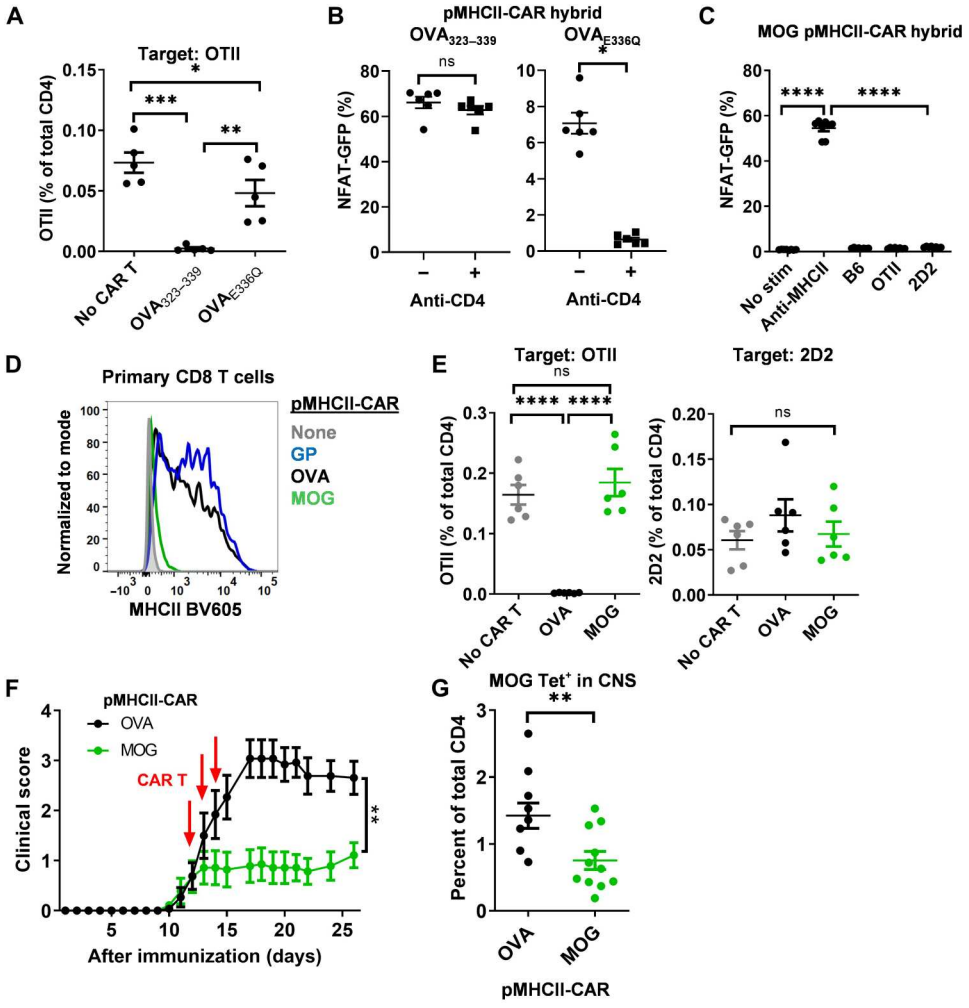

Fig. 3. Treatment of EAE with $MOG_{35–55}$ pMHCII-CAR T cells. (**A**) Decreased OTII T cell depletion with lower-affinity pMHCII-CAR T cells. B6 mice were injected with 2×10^5 OTII cells, followed the next day by 2×10^5 $OVA_{323–339}$ or OVA_{E336Q} pMHCII-CAR T cells. The frequency of OTII cells among the total $CD4^+$ T cell population was assessed 5 days after CAR T injection by flow cytometry (expt. = 2; $n = 4$ or 5 per group). (**B**) CD4 co-receptor involvement in low-affinity pMHCII-CAR signaling. OVA pMHCII-CAR hybrids were cocultured with OTII cells in the presence or absence of anti-CD4 (20 μg/ml) for 2 days and assessed for NFAT-GFP by flow cytometry (expt. = 2; each with three technical replicates). (**C**) $MOG_{35–55}$ pMHCII-CAR hybridomas do not recognize 2D2 in vitro. $MOG_{35–55}$ pMHCII-CAR hybridoma cells were cocultured with the indicated naïve T cells. NFAT-GFP expression was examined after 2 days by flow cytometry (expt. = 2; each with three technical replicates). Plate-coated anti-MHCII antibody (20 μg/ml) was used as positive control. (**D**) Low expression of $MOG_{35–55}$ pMHCII-CAR on primary $CD8^+$ T cells by flow cytometry. Surface expression of $OVA_{323–339}$ and $GP_{61–80}$ pMHCII-CAR is shown for comparison. Events shown are gated on $Thy1.1^+$-transduced cells. (**E**) Inability to deplete 2D2 TCR Tg T cells with $MOG_{35–55}$ pMHCII-CAR T cells in vivo. OTII and 2D2 TCR Tg T cells (2×10^5 each) were coinjected 1 day before injection of 2×10^5 pMHCII-CAR T cells. At day 5 after CAR T cell injection, the percentages of OTII (left) or 2D2 T cells (right) of total $CD4^+$ T cells were assessed as $V\alpha2^+V\alpha3.2^-$ or $V\alpha2^-V\alpha3.2^+$, respectively, of transferred $CD45.1^+$ $CD4^+$ T cells by flow cytometry (expt. = 2; $n = 6$ per group). (**F** and **G**) Amelioration of EAE with $MOG_{35–55}$ pMHCII-CAR T cells. EAE was induced by immunization with $MOG_{35–55}$ in FCA with two doses of PTX separated by 48 hours, followed by 3×10^6 $OVA_{323–339}$ or $MOG_{35–55}$ pMHCII-CAR T cells injected at days 12, 13, and 14 after immunization. (F) Disease activity was assessed by a clinical score for neurologic impairment (expt. = 2; $n = 13$ or 14 per group). (G) Flow cytometric analysis of $MOG_{38–49}$ tetramer$^+$ (Tet^+) cells in the CNS at day 26 after immunization (expt. = 2; $n = 10$ or 11 per group). *P* values were determined by nested Student's *t* test (B), ordinary Student's *t* test (G), nested ANOVA with Holm-Sidak (C), ordinary ANOVA with Holm-Sidak (A and E), or repeated-measures ANOVA (F). Bars show means ± SEM; $^*P < 0.05$; $^{**}P < 0.01$; $^{***}P < 0.001$; $^{****}P < 0.0001$.

(Fig. 5F). We also asked whether MOG-specific CAR T cells could inadvertently cause neurotoxicity (*31*) when treating ongoing EAE later in the disease course (day 18 after immunization) via the use of a slightly modified EAE protocol with reduced severity (*32*). We did not see evidence as a group or in individual mice of clinical worsening after CAR T cell administration (fig. S5). Consistent with superiority at clinical onset (Fig. 5F), we observed a therapeutic effect of MOG_{DST} pMHCII-CAR-$Fas^{\Delta DD}$ but not $MOG_{35–55}$ CAR T cells on established EAE (Fig. 5G and fig. S5), which was associated with significantly improved CAR T survival in the CNS (Fig. 5H). Collectively, these data provide a proof of principle that antigen-specific CAR T cells can be used to treat ongoing autoimmune disease.

Targeting lower-affinity MOG-specific T cells is critical for amelioration of EAE

Although we inferred that the ability of MOG_{DST} pMHCII-CAR-$Fas^{\Delta DD}$, but not $MOG_{35–55}$ pMHCII-CAR, T cells to treat EAE is

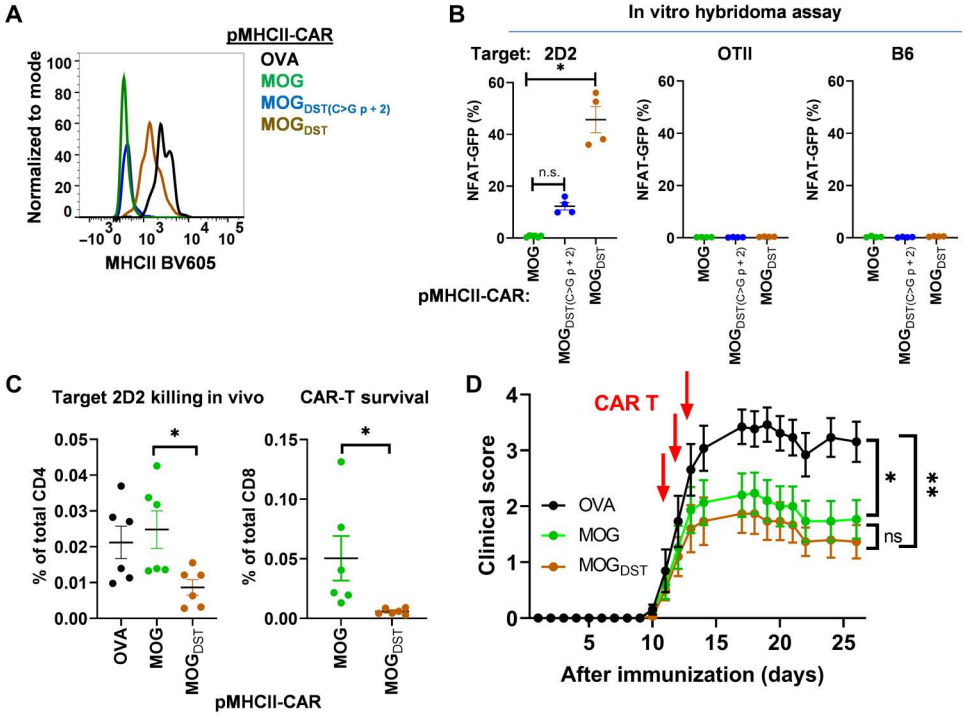

Fig. 4. DST modification improves MOG pMHCII-CAR surface expression and sensitivity. (**A**) Surface expression of indicated pMHCII-CAR by flow cytometry of transduced primary CD8$^+$ T cells. (**B**) MOG_{DST} pMHCII-CAR recognizes 2D2 TCR in vitro. NFAT-GFP expression at 2 days was assessed using hybridoma cells expressing a pMHCII-CAR (indicated on the *x* axis) cocultured with the naïve T cells (top of graph) (expt. = 2; each with two technical replicates). (**C**) 2D2 target T cell deletion by MOG_{DST} pMHCII-CAR T cells. 2D2 TCR Tg cells (2×10^5) were injected 1 day before injection of the indicated 2×10^5 pMHCII-CAR T cells. Shown are 2D2 target (left) or CAR (right) T cell survival as a percentage of total CD4$^+$ or CD8$^+$ T cells 5 days later (expt. = 2; $n = 6$ per group). (**D**) No significant improvement in EAE therapy with MOG_{DST} pMHCII-CAR T cells. EAE induction and CAR T cell therapy was performed as per Fig. 3F, with 3×10^6 pMHCII-CAR T cells injected at days 11 to 13 after immunization (expt. = 2; $n = 13$ to 15 per group). *P* values were determined by nested one-way ANOVA with Holm-Sidak multiple comparison (B), ordinary ANOVA with Holm-Sidak (C), or repeated-measures ANOVA (D). Bars show means ± SEM; $*P < 0.05$; $**P < 0.01$.

a result of lower-affinity MOG-specific T cell deletion, this was only on the basis of a differential effect in 2D2 cell killing. To obtain greater insight regarding the TCRs targeted by these pMHCII-CARs, we studied their impact on the MOG-specific TCR repertoire of fixed TCRβ chain TCliβ Tg mice (Fig. 6A) (*12*, *17*, *18*, *33*). We first identified putative MOG-specific TCRs in TCRβ Tg mice by performing TCRα sequencing of Foxp3$^{IRES\text{-}GFP-}$ CD44^{hi} CD62L^{lo} T effector (Teff) cells sorted from mice immunized in vivo with $MOG_{35–55}$ and further expanded in vitro on splenic DCs and MOG peptide (Fig. 6, B and C). Many of the in vitro expanded TCRs were commonly found in the Teff subset in the CNS of mice with clinical EAE, supporting the notion that they are MOG specific (Fig. 6D). Last, we asked whether we could identify any TCRs that were removed from the CNS due to $MOG_{35–55}$ pMHCII-CAR T cells. By DESeq2 analysis, we found three abundant T_{reg}, but not Teff, TCRs that were decreased in frequency with CAR T treatment (Fig. 6E). In summary, we picked three CNS T_{reg} TCRs and eight TCRs identified in our in vitro assay for functional testing of MOG reactivity (Fig. 6F).

These 11 TCRα chains were gene-synthesized and retrovirally expressed on NFAT-GFP reporter hybridoma cells expressing the fixed TCRβ chain and murine CD4 (*12*, *17*, *18*). Eight TCRs were stimulated by $MOG_{35–55}$ presented by FMS-like tyrosine kinase 3 ligand (flt3L)–induced DCs with widely varying efficiencies as measured by an estimated EC_{50} (half-maximal effective concentration) and used here as a surrogate for pMHCII-TCR affinity (Figs. 6F and 7A). There was a strong bias toward a single CDR3 length and two different J chains among the MOG-reactive TCRs, with the exception of JYM14, the TCR with the highest reactivity (Fig. 6F). In summary, this approach allowed us to capture a substantial fraction of the MOG-specific TCR repertoire in TCliβ Tg mice, which spans an estimated thousand-fold range of "affinity" for $MOG_{35–55}$ (Figs. 6F and 7A).

Of this group of MOG-reactive TCRs, the two TCRs with the highest sensitivity (JYM14 and DS4) were enriched in T_{regs} in the CNS of EAE mice, whereas the remaining TCRs were predominantly found in the Teff subset (Fig. 7B). This is consistent with prior modeling of thymic T_{reg} development (*16*) and studies of MOG-specific T cells (*34*). We observed a strong inverse correlation between the frequency of MOG-specific Teff TCRs in the CNS and sensitivity to $MOG_{35–55}$ peptide (Fig. 7C), indicating that lower-affinity, and not higher-affinity, MOG-specific T cells represent the majority of CNS infiltrating Teff cells during EAE. These lower-affinity MOG-specific TCR frequencies were markedly higher in the CNS than peripheral LN (PLN) (fig. S6). Preferential expansion of lower-affinity MOG-specific Teff TCRs was also observed in TCR repertoire studies between weeks 2 and 4 in the PLN (Fig. 7D). Together, these data strongly suggest that, during the EAE disease course, there is progressive selection toward lower-affinity MOG-specific effector TCR clones.

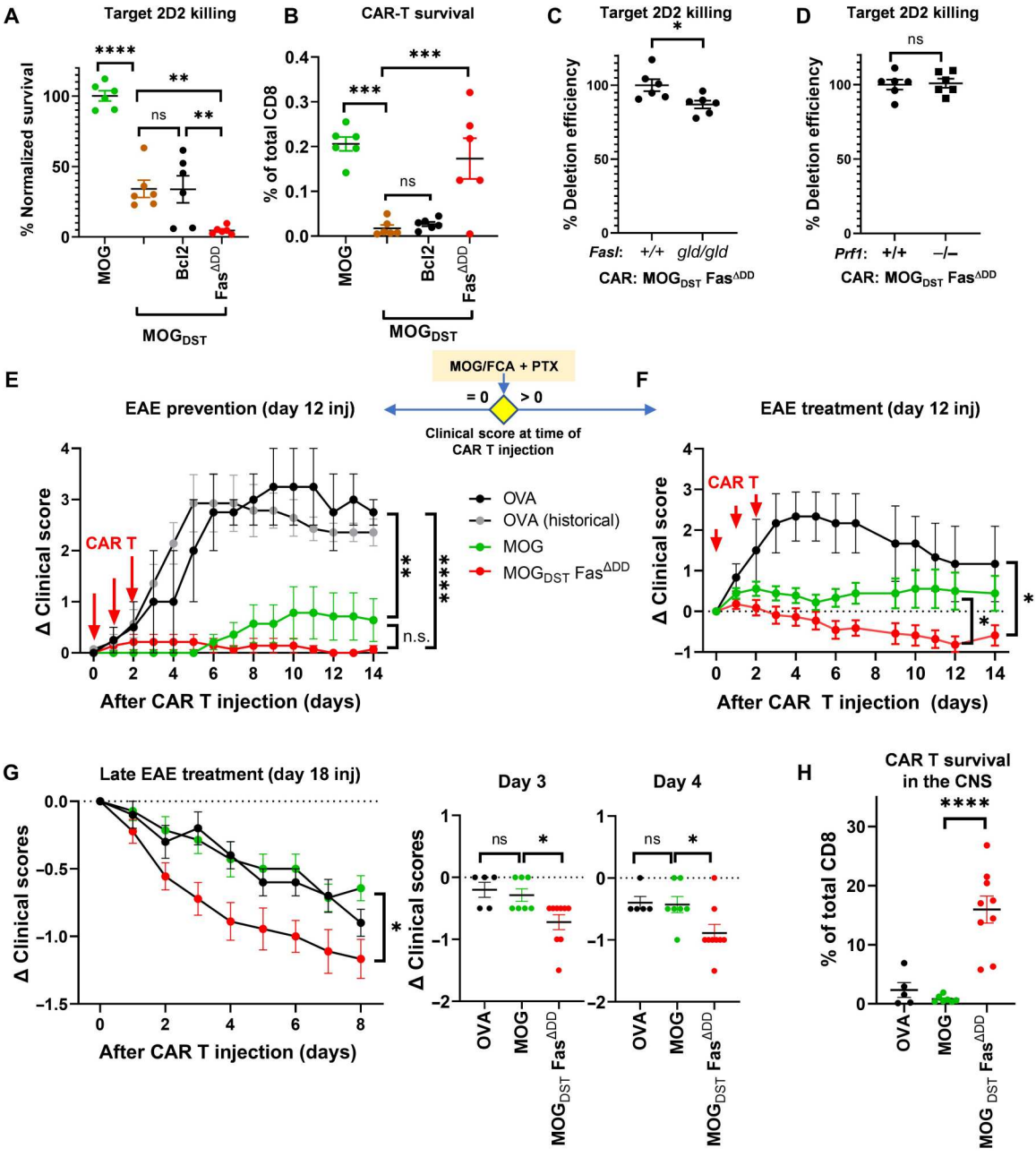

Fig. 5. Fas blockade on pMHCII CAR T cells improves target T cell killing and EAE treatment. (**A** and **B**) Efficient in vivo depletion of 2D2 cells by MOG_{DST} pMHCII-$Fas^{\Delta DD}$-CAR T cells. Congenitally marked target 2D2 and OTII cells (2×10^5 each) were cotransferred 1 day before injection of indicated 2×10^5 pMHCII-CAR T cells (*x* axis) and assessed 5 days later (expt. = 2; *n* = 6 per group). Shown are (A) 2D2 survival represented by its ratio to the internal OTII injection control, which is then normalized to 100% survival in the $MOG_{35–55}$ pMHCII-CAR no-deletion control samples, and (B) percentage of surviving CAR T cells of total $CD8^+$ cells. (**C** and **D**) Assessment of pMHCII-CAR T cell–mediated killing mechanisms. *Fasl*^{gld} (C) or *Prf1*$^{-/-}$ (D) $CD8^+$ T cells were used to generate MOG_{DST} pMHCII-$Fas^{\Delta DD}$-CAR T cells. Shown is the target 2D2 T cell deletion efficiency at day 3 after CAR T cell injection normalized to the WT condition (expt. = 2; *n* = 6 per group). (**E** and **F**) Improved EAE treatment by MOG_{DST} pMHCII-$Fas^{\Delta DD}$-CAR T cells. EAE was induced as per Fig. 3F. The indicated pMHCII-CAR T cells (3×10^6) were injected at days 12 to 14 after immunization. (E) EAE prevention represents mice with clinical score = 0 at time of CAR T cell injection [expt. = 2; *n* = 7 $MOG_{35–55}$, 7 MOG_{DST} pMHCII-$Fas^{\Delta DD}$, 2 OVA, and 7 OVA (historical, expt. = 2)]. (F) EAE treatment represents data from mice with a clinical score of >0 at the time of CAR T cell therapy (expt. = 2; *n* = 3 OVA, 9 $MOG_{35–55}$, and 11 $MOG_{DST}Fas^{\Delta DD}$). Data shown are the Δ from the clinical score on day of CAR T cell injection. (**G** and **H**) Treatment of established EAE with CAR T cells (see also fig. S5). Data shown are (G) the Δ from the clinical score on day of CAR T cell injection (day 18), and (H) CAR T cell survival in the CNS 8 days after injection (expt. = 2; *n* = 5 OVA, 7 $MOG_{35–55}$, and 9 $MOG_{DST}Fas^{\Delta DD}$). To assess both the utility and potential toxicity of CAR T cells on moderate EAE, we analyzed mice with clinical scores of 1.5 to 2.5 on day 18 after immunization. Student's *t* test or one-way ANOVA with Holm-Sidak (A to D and H) or repeated-measures ANOVA (E to G). Kruskal-Wallis test for day 3 or 4 graphs on right of (G). Bars show means ± SEM; *$P < 0.05$; **$P < 0.01$; ***$P < 0.001$; ****$P < 0.0001$.

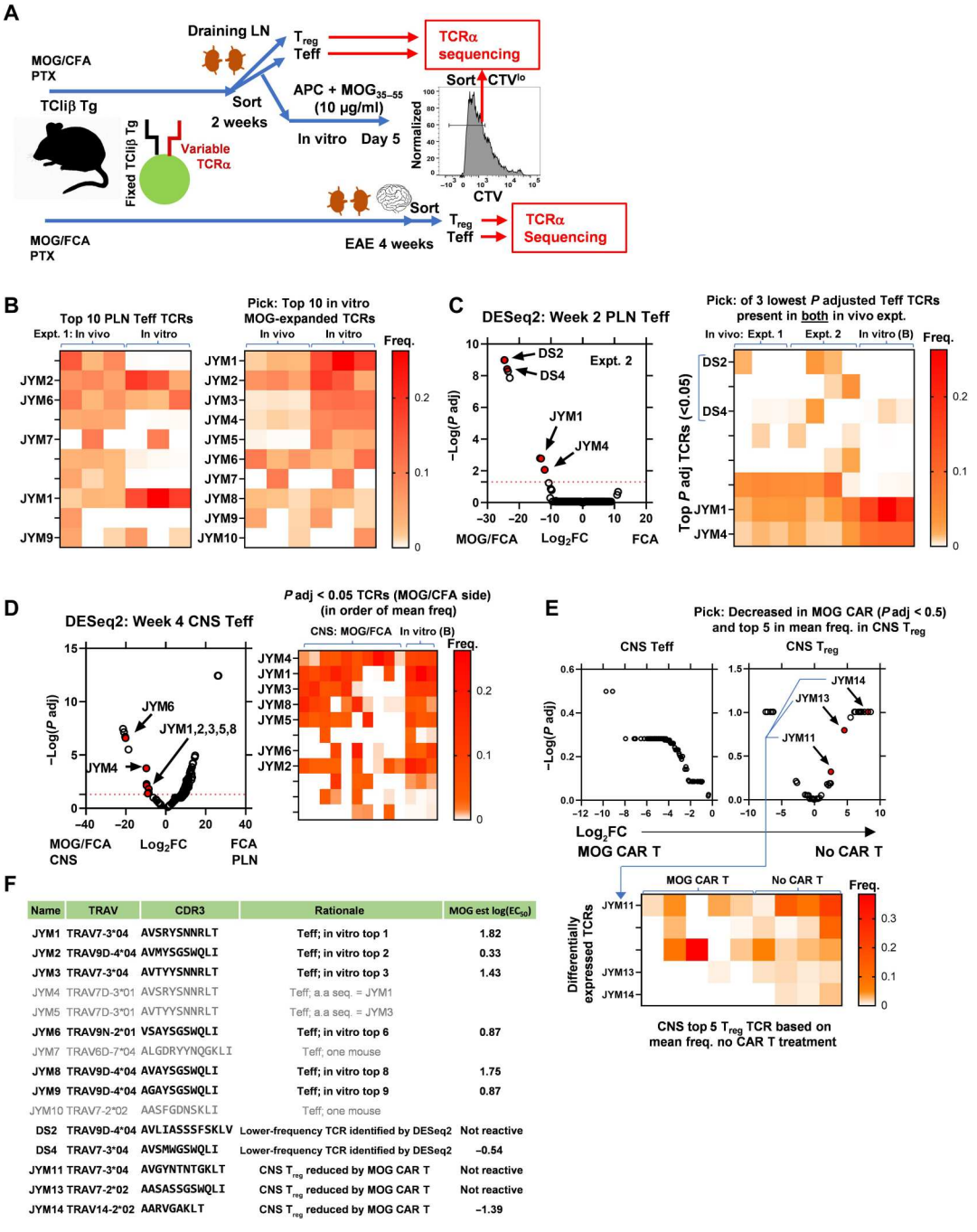

F

Name	TRAV	CDR3	Rationale	MOG est log(EC50)
JYM1	TRAV7-3*04	AVSRYSNNRLT	Teff; in vitro top 1	1.82
JYM2	TRAV9D-4*04	AVMYSGSWQLI	Teff; in vitro top 2	0.33
JYM3	TRAV7-3*04	AVTYYSNNRLT	Teff; in vitro top 3	1.43
JYM4	TRAV7D-3*01	AVSRYSNNRLT	Teff; a.a seq. = JYM1	
JYM5	TRAV7D-3*01	AVTYYSNNRLT	Teff; a.a seq. = JYM3	
JYM6	TRAV9N-2*01	VSAYSGSWQLI	Teff; in vitro top 6	0.87
JYM7	TRAV6D-7*04	ALGDRYYNQGKLI	Teff; one mouse	
JYM8	TRAV9D-4*04	AVAYSGSWQLI	Teff; in vitro top 8	1.75
JYM9	TRAV9D-4*04	AGAYSGSWQLI	Teff; in vitro top 9	0.87
JYM10	TRAV7-2*02	AASFGDNSKLI	Teff; one mouse	
DS2	TRAV9D-4*04	AVLIASSSFSKLV	Lower-frequency TCR identified by DESeq2	Not reactive
DS4	TRAV7-3*04	AVSMWGSWQLI	Lower-frequency TCR identified by DESeq2	−0.54
JYM11	TRAV7-3*04	AVGYNTNTGKLT	CNS Treg reduced by MOG CAR T	Not reactive
JYM13	TRAV7-2*02	AASASSGSWQLI	CNS Treg reduced by MOG CAR T	Not reactive
JYM14	TRAV14-2*02	AARVGAKLT	CNS Treg reduced by MOG CAR T	−1.39

Fig. 6. Selection of candidate MOG-specific TCR clones from TCR repertoire analysis. (**A**) Experimental strategy for TCR sequencing with TCliβ Tg *Foxp3*$^{IRES\text{-}GFP}$ mice. Mice were immunized with $MOG_{35–55}$ in FCA followed with two doses of PTX. TCRα sequencing was performed with purified PLN T_{regs} or Teff cells at week 2 or with PLN or CNS T cells at week 4. For in vitro expansion, week 2 PLN Teff cells were labeled with CellTrace Violet (CTV) and cocultured with splenic DCs for 5 days in the presence of $MOG_{35–55}$ peptide (10 μg/ml), and then CTV^{-} cells were sorted for TCR sequencing. (**B**) Selection of in vitro expanded TCRs. Heatmaps show frequencies of top 10 Teff TCRs from in vivo week 2 PLN (left) or further expansion in vitro (right) (expt. = 1; $n = 3$). (**C**) Selection of lower-frequency TCR DS2 and DS4 on the basis of DESeq2 analysis with week 2 PLN Teff TCR repertoire after mice were immunized with FCA or MOG/FCA. Volcano plot (left) shows differentially induced TCRs. Dots indicate individual TCRs. Dashed red line indicates *P* adjusted = 0.05 from DESeq2. Heatmap (right) shows frequencies of top *P*-adjusted TCRs (expt. = 1; $n = 4$ per group). (**D**) Top CNS Teff TCRs at week 4 in EAE mice. Volcano plot shows differentially induced CNS Teff TCRs (left; expt. = 2; $n = 10$) when compared with PLN data of FCA-immunized mice of (C). Heatmap (right) shows frequencies of top CNS Teff TCRs versus in vitro expanded TCRs. (**E**) Selection of CNS T_{reg} TCRs JYM11, JYM13, and JYM14 that may be reduced by $MOG_{35–55}$ pMHCII-CAR T cells. TCR repertoire analysis was performed with Teff cells or T_{regs} from the CNS of TCliβ Tg *Foxp3*$^{IRES\text{-}GFP}$ mice at week 4 as per (A), except the mice received media or 3×10^7 total $MOG_{35–55}$ pMHCII CAR T cells at days 7 to 9. Volcano plots (top) of Teff or T_{reg} TCR repertoire when comparing no CAR T and $MOG_{35–55}$ CAR T group (expt. = 1; $n = 4$ to 5 per group). Heatmap (bottom) shows frequencies of top five CNS T_{reg} TCRs. Among these, TCRs potentially reduced in frequency by $MOG_{35–55}$ CAR T cells (relaxed criteria of *P* adjusted < 0.5) were selected for functional testing. (**F**) Candidate MOG-specific TCRs tested. Shown are rationales for selecting each TCR and their reactivity to $MOG_{35–55}$ peptide.

We next asked whether pMHCII-CAR T cell treatment altered the MOG-specific TCR repertoire. Although EAE was milder likely because of the limited TCR repertoire in fixed TCRβ chain Tg mice, a clear inhibition of EAE was mediated by $MOG_{35–55}$ pMHCII-CAR and MOG_{DST} pMHCII-CAR-$Fas^{\Delta DD}$ T cells (fig. S7A). Although there was not an obvious change in α diversity of the CNS Teff TCR repertoire with CAR T cell therapy (fig. S7B), a nonmetric multidimensional scaling (NMDS) plot showed that MOG_{DST} pMHCII-CAR-$Fas^{\Delta DD}$ induced greater changes in the CNS Teff TCR repertoire than $MOG_{35–55}$ pMHCII-CAR (Fig. 7E), which is supported by permutational multivariate analysis of variance (PERMANOVA) testing (Fig. 7F), DESeq2 differential expression analysis (fig. S7C), and the cumulative loss of $MOG_{35–55}$-specific TCRs (Fig. 7, G and H, and fig. S7D). Thus,

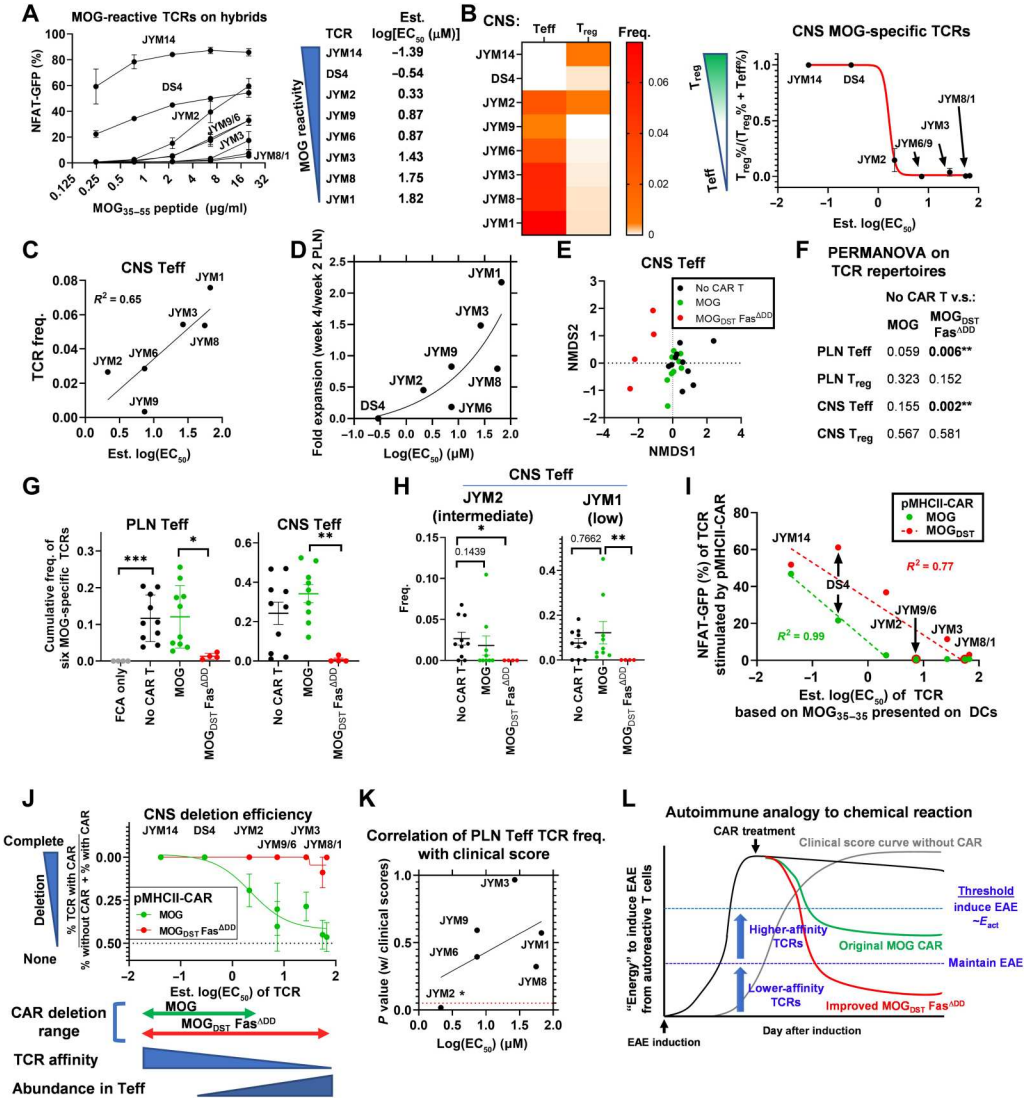

Fig. 7. Targeting lower-affinity MOG-specific T cells is required for amelioration of EAE. (**A**) MOG reactivities of TCRs identified by TCR repertoire analysis in Fig. 6. Data shown are percentage of NFAT-GFP$^+$ of the indicated TCR-expressing hybridoma cells in response to titrated doses of $MOG_{35–55}$ peptide presented by flt3L-stimulated DCs after 2 days. These curves were used to estimate an EC_{50} (right). Note that the EC_{50} of very low-reactivity TCRs is extrapolated. No peptide controls showed <1% NFAT-GFP (expt. = 2; four technical replicates). (**B**) Correlation between TCR affinity and T cell subset. Left: Heatmap of mean T_{reg} or Teff TCR frequency in the CNS of EAE-induced mice at 4 weeks of individual MOG-specific TCRs arranged in order of decreasing reactivity based on (A). Right: Skewing towards the T_{reg} versus Teff subset is shown [% in T_{reg} repertoire/(% in T_{reg} repertoire + % in Teff repertoire)]. Red line is derived from sigmoidal fitting analysis. (**C**) Correlation between TCR affinity and abundance in CNS Teff TCR repertoire at week 4. Black line is from linear regression. (**D**) Correlation between EC_{50} and fold increase of individual MOG-specific TCR between weeks 2 and 4 in PLN Teff TCR repertoire. The line is nonlinear sigmoidal fitting. (**E** and **F**) MOG_{DST} pMHCII-Fas$^{\Delta DD}$-CAR T cells, but not $MOG_{35–55}$ pMHCII-CAR T cells, induce significant changes in the TCR repertoire experiments described in Fig. 6E and fig. S5. Data shown are NMDS plots of horn distance for CNS Teff TCRs at week 4 (E) and *P* values of PERMANOVA tests between the indicated samples (F). Each dot represents data from individual mice. (**G** and **H**) Deletion of MOG-specific TCRs by pMHCII-CAR T cells. Each dot represents data from individual mice. (G) The cumulative frequencies of six known MOG-reactive Teff TCRs are shown from the PLN or CNS Teff subset with the indicated pMHCII-CAR T cell treatment. (H) Individual intermediate-affinity (JYM2) or lower-affinity (JYM1) TCR frequencies in the CNS Teff cells are shown. Also see fig. S5D. (**I**) Correlation of TCR activation by pMHCII-CAR and $MOG_{35–55}$ peptide. Percentages of NFAT-GFP$^+$ cells of TCR-transduced hybridoma cells interacting with indicated pMHCII-CAR–expressing hybridoma cells were correlated with estimated EC_{50} from (A). Green ($MOG_{35–55}$) or red (MOG_{DST}) lines are from simple linear regression of points on the linear portion of the curve (top three for MOG and all points for MOG_{DST}). (**J**) Model integrating TCR affinity, autoimmunity, and pMHCII-CAR deletion. Correlation between TCR affinity and pMHCII-CAR–mediated depletion efficiency is shown. Red ($MOG_{DST}FAS^{\Delta DD}$) or green ($MOG_{35–55}$) lines represent sigmoidal fitting of deletion efficiency. Abundant MOG-specific Teff cells are of relatively lower affinity. $MOG_{35–55}$ pMHCII-CAR T cells can eliminate higher-affinity MOG-specific T cells, whereas deletion of lower-affinity MOG-specific Teff cells requires MOG_{DST} pMHCII-CAR-Fas$^{\Delta DD}$ T cells. (**K**) Correlation of higher-affinity Teff TCR JYM2 with disease severity in $MOG_{35–55}$ pMHCII-CAR T cell–treated mice. *P* values are from Spearman's correlation between clinical scores and MOG-specific TCR frequencies in PLN Teff cells. (**L**) Hypothetical activation energy (E_{act}) model for induction of autoimmunity. The role of higher-affinity MOG-specific T cells in EAE may be analogous to activation energy in a chemical reaction, whereas once autoimmunity is initiated, it can be maintained by lower-affinity T cells. The gray line indicates clinical score, which would be on a different *y* axis scale and would lag behind the activation energy (black line) needed to induce disease. Kruskal-Wallis test (G and H); *$P < 0.05$; **$P < 0.01$; ***$P < 0.001$.

these data demonstrate that MOG_{DST} pMHCII-CAR-Fas$^{\Delta DD}$ T cells deleted the vast majority of MOG-specific Teff cells in the CNS (Fig. 7G and fig. S7D), which correlated with the efficiency of TCR:pMHCII-CAR interaction (Fig. 7, H to J).

The frequency of the higher-affinity MOG-specific Teff TCR, JYM2, remaining within the PLN ~3 weeks after $MOG_{35–55}$ pMHCII-CAR T cell treatment was significantly correlated with the clinical score (Fig. 7K), whereas the frequencies of lower-affinity TCRs were not correlated. We found about twofold higher sensitivity of JYM2 TCR to $MOG_{35–55}$ peptide when compared with 2D2 TCR (fig. S7E). Together, the TCR repertoire and 2D2 killing data support the conclusion that generation of lower-affinity MOG-specific T cells without higher-affinity T cells does not lead to the development of clinical disease. These data therefore suggest

that the generation of higher-affinity T cells is analogous to the provision of "activation energy" in a chemical reaction, which is required to initiate autoimmunity, whereas lower-affinity T cells are sufficient for the maintenance of ongoing autoimmunity (Fig. 7L).

DISCUSSION

Our data are consistent with recent reports regarding the potential for antigen-specific T cell depletion therapy for autoimmunity. For example, in a partially humanized murine model of rheumatoid arthritis, pMHCII-CAR T cells composed of HLA-DR1 bound to a type II collagen peptide were effective at preventing collagen-induced arthritis (*35*). The pMHCII-CAR approach represents an alternative to a recent report using a MHCII-TCR fusion (5M)CAR to prevent autoimmune diabetes (*23*). A potential advantage of using the intact MHCII molecule over a MHCII-TCR fusion is the ease of constructing pMHCII-CARs using different MHCII alleles, which we did with murine I-A^d and human HLA-DR4 sequences without modification as proof of principle. On the other hand, the MHCII-TCR fusion has a theoretical advantage via the use of endogenous CD3 signaling mechanisms compared with the 28z in our pMHCII-CAR. However, the signaling domain of pMHCII-CAR can be further tuned to increase or decrease sensitivity, whereas the MHC-TCR:CD3 signal cannot be easily adjusted. Moreover, the MHCII-TCR fusion does not result in CD4 co-receptor engagement, requiring addition of nonspecific co-receptors with signaling domains (CD80-lck). Future experiments will be required to directly compare these methodologies and evaluate the efficiency of TCR recognition, $CD4^+$ T cell killing, and CAR T cell persistence.

One challenge that we encountered regarding antigen-specific therapy for autoimmunity is that the affinity of self-reactive Teff cells appears substantially lower than those reactive to foreign antigens, presumably due to the need to escape thymic negative and T_{reg} selection (*19*). Consequently, higher-affinity self-reactive T_{regs} are likely to be preferentially eliminated. Our TCR repertoire analysis confirmed that MOG-specific T_{reg} TCRs were higher affinity than Teff TCRs (*34*) and are preferentially eliminated by the lower-sensitivity $MOG_{35–55}$ pMHCII-CAR T cells, whereas a substantial number of MOG-specific Teff cells remain. However, the lack of disease exacerbation suggests that a proposed T_{reg} suppression mechanism based on peptide-specific inhibition (*36*) may not be essential to abrogate inflammation. Rather, our data are supportive of a recent study of prostate antigens (*37*) arguing against this requirement for T_{reg} function. Future studies will be required to ascertain the importance of T_{reg} elimination with pMHCII-CAR T cell therapy. By contrast, selective elimination of antigen-specific T_{regs} using lower-sensitivity pMHCII-CAR T cells may be of benefit for cancer immunotherapy.

One unexpected finding from the TCR repertoire analysis was that lower-affinity, and not higher-affinity, MOG-specific TCRs expanded in the PLN between weeks 2 and 4 after MOG immunization. In addition, we found an inverse correlation between affinity and abundance of MOG-specific Teff TCRs in the CNS. This is similar to a study of chronic cytomegalovirus infection (*38*) and in line with previous observations supporting a greater role of lower-affinity T cells in EAE and other responses (*8*, *39*). Our data are consistent with the literature showing that $MOG_{35–55}$-specific T_{reg} TCRs are of substantially higher affinity for self than Teff cells (*34*), that 2D2 cells exhibit "low" affinity for MOG (*9*), and that many MOG-specific TCRs may lie below the detection range of pMHCII tetramers based on 2D affinity measurements (*8*). Initial attempts to treat EAE with a $MOG_{35–55}$ pMHCII-CAR were successful in preventing EAE from worsening but could not improve clinical signs of ongoing disease. Addressing the durability of $MOG_{35–55}$ CAR T cell responses during certain stages of disease remains as an important future question. Improvements in pMHCII-CAR stability and signaling strength via the use of a DST, and prevention of CAR T cell death via the use of a dominant-negative $Fas^{\Delta DD}$, resulted in higher sensitivity that allowed the targeting of both higher- and lower-affinity MOG-specific $CD4^+$ T cells. The difference between the original lower-sensitivity and improved higher-sensitivity MOG pMHCII CARs enabled us to investigate the relative contributions of higher-affinity versus lower-affinity T cells in ongoing autoimmune disease.

The observations using pMHCII-CAR T cells with differential sensitivity for self-reactive TCRs lead us to propose a model whereby higher-affinity autoreactive T cells provide initial activation energy to initiate autoimmunity, analogous to the energy required to initiate a chemical reaction. We postulate that previously reported driver clones (*40*) represent higher-affinity T cells, providing activation energy for initiating autoimmune disease. This model suggests that autoimmune disease is difficult to trigger, because thymic selection or peripheral expansion of high-affinity self-reactive T cells would occur inefficiently. Although further studies are required to extend these results beyond the active EAE model studied here, our results imply that the elimination of infrequently generated high-affinity autoreactive T cell clones with pMHCII-CAR T cell treatment may be sufficient to prevent onset of autoimmune disease if this threshold has not been crossed.

The notion of a "prodrome" phase before crossing the activation energy threshold into autoimmune disease has been observed in both mouse models and humans. For example, it is well established that nonobese diabetic mice invariably develop a clear inflammatory reaction around the islets of Langerhans at a young age, but islet destruction develops later (*41*). In humans, this may be analogous to the observation that autoantibodies to insulin are detectable well before development of diabetes (*42*, *43*). Similarly, antinuclear and antithyroid antibodies can be observed well before the diagnosis of systemic lupus erythematosus or autoimmune thyroiditis (*44*, *45*). Thus, these examples support the model that an activation energy threshold is required for the development of autoimmune pathology.

Last, our model of autoimmunity suggests that lower-affinity T cells are sufficient to perpetuate disease activity. This would therefore imply that targeting flares of disease may not be sufficient to mitigate long-term damage due to persistence and activity from lower-affinity T cells. The benefit of curtailing clinical relapses in MS, for example, is controversial, because current disease-modifying therapies are highly effective at reducing relapse rates but are not as effective at preventing eventual progression of disability (*46*), perhaps analogous to our treatment with lower-sensitivity pMHCII-CAR T cells. Thus, we speculate that targeting the repertoire of low-affinity autoreactive T cells driving chronic smoldering CNS inflammation may address a key underlying driver of MS disability. Although our most modified CAR T cells showed significant therapeutic effect on ongoing disease, we were not able to completely resolve clinical outcomes, which implies that further

modifications are required, such as engineering homing receptors, increasing/decreasing sensitivity of signaling domain, and incorporating other genes to help cytotoxicity and survival. Last, targeting additional peptide specificities emerging from epitope spreading could be a promising strategy for efficient treatment of autoimmunity.

MATERIALS AND METHODS

Study design

The aim of this study was to specifically eliminate autoreactive T cells using pMHCII-CAR–expressing $CD8^+$ T cells. During the development of pMHCII-CAR constructs with greater functional capacity, we sought to understand the role of higher- and lower-affinity self-reactive TCRs during autoimmunity. The efficacy of pMHCII-CAR constructs was assessed using various approaches, including in vitro NFAT-GFP cell line assays, in vivo depletion assays using Tg $CD4^+$ T cells, the active EAE mouse model of autoimmunity, and TCR sequencing analysis.

Mice

Mouse breeding and experiments were performed in a specific pathogen–free facility using protocols approved by the Washington University Animal Studies Committee. Strains used (table S1) are the following: C57BL/6 and Balb/c mice were obtained from Charles River Laboratories or the Jackson Laboratory. OT-II (#004194), SMARTA (# 030450), 2D2 (#006912), and CD45.1 C57BL/6 (#002014), *Prf1*$^{-/-}$ (#002407), and *FasL*^{gld} (#001021) mice were obtained from the Jackson Laboratory. TCli TCRαβ mice were previously described (*33*). Each TCR Tg line was maintained as CD45.1 C57BL/6 background. DO11 mice were provided by K. Murphy (Washington University School of Medicine in St. Louis). TCli TCRβ mice (*33*) were bred with *Tcra*$^{-/-}$ (the Jackson Laboratory, #002116) and *Foxp3*$^{IRES\text{-}GFP}$ mice (the Jackson Laboratory, #006772). TCli TCRβ *Tcra*$^{+/-}$ *Foxp3*$^{IRES\text{-}GFP}$ mice were used for TCR sequencing as previously described (*18*). Six- to 8-week-old male and female mice were used for experiments with the exception of mice used for active EAE induction, which were 8- to 10-week-old male and female mice.

pMHCII-CAR constructs

We first tested MigR1-based retroviral (RV) constructs in which a second-generation 28z signaling domain was attached immediately after the TM domain or after the C terminus of either the I-A^b α or β chain. To facilitate surface expression, we added a peptide with a 16–amino acid flexible linker after the signal peptide in I-A^b β as previously described (*13*). To facilitate transduction of primary T cells, we generated a tricistronic RV vector with signal peptide-antigen peptide-linker-I-A^bβ-28z-(GSG)P2A-I-A^bα with an internal ribosomal entry site (IRES)–Thy1.1 (or mCherry) reporter. I-A^b α and β sequences were replaced for different MHC or HLA alleles. The DST was generated as described (*26*) with a cysteine amino acid after the peptide in the p9 + 2 position or a glycine as a control. In some experiments, Bcl2 (*47*) or $Fas^{\Delta DD}$ (*28*) was added after the I-A^b α with a (GSG)T2A sequence. Please refer to Fig. 1C and table S2.

RV production

RV was produced as previously described (*48*). Briefly, MigR1-based RV vectors were transfected into Phoenix-Ecotropic cell line using TransIT-293 (Thermo Fisher Scientific, #MIR2700). Viral supernatant was collected after culturing cells at 32°C for 24 hours.

In vitro NFAT-GFP hybridoma assay

For measuring pMHCII-CAR reactivity to TCR Tg T cells, NFAT-GFP hybridoma assays were performed as previously described (*12*). Briefly, hybridoma cells expressing GFP under an NFAT promoter were retrovirally transduced with pMHCII-CAR vectors. RV transduced hybridoma cells (10^4) were cocultured for 2 days with primary target TCR T cells (2×10^5) before assessment of GFP expression. As a positive control, wells were coated with anti-MHCII antibody (20 μg/ml; Bio X Cell; clone M5/114) or anti–HLA-DR (20 μg/ml; Bio X Cell, clone L243). For measuring sensitivity of cloned TCR to $MOG_{35–55}$ peptide, TCRα chains were gene-synthesized and retrovirally expressed on NFAT-GFP reporter hybridoma cells expressing the fixed TCRβ chain and murine CD4 (*12*, *17*). A total of 1×10^4 TCR-expressing lines were cocultured for 2 days with 2.5×10^4 flt3L-stimulated DCs in the presence of titrated concentrations of $MOG_{35–55}$ peptide (0.25 to 20 μg/ml) before analysis of GFP expression. To assess interaction between the MOG pMHCII-CAR construct and MOG-specific TCRs, we cocultured each 1×10^4 MOG pMHCII-CAR–expressing cell line and 1×10^4 TCR-expressing line for 2 days before GFP measurement on TCR-expressing lines.

In vitro NFAT-GFP Jurkat assay

The NY-ESO-1–targeted TCR (*15*) was provided by T. Blankenstein (Max Delbrück Center for Molecular Medicine, Berlin, Germany). $TRAC^{KO}$/$TRBC^{KO}$ dual knockout (KO) Jurkat cells engineered to express an NFAT-GFP reporter (*14*) were engineered to express NY-ESO-$1_{119–133}$ or $MOG_{97–108}$ pMHCII(DR4)-CARs (*15*). Transduction efficiency was assessed by flow cytometry using an anti-DR4 antibody (BioLegend, clone L243). In parallel, dual KO Jurkat cells were engineered to express a Tg TCR-targeting NY-ESO-$1_{119–133}$, and transduction efficiency was evaluated by flow cytometry using an anti-TCR constant chain antibody (Invitrogen, clone WT31). Cocultures were established at effector (CAR^+)–to–target (TCR^+) ratios of 1:4, and the GFP signal in CAR^+ cells was assessed after 18 hours.

pMHCII-CAR T cell generation and transfer

Fluorescence-activated cell sorting (FACS)–purified $CD44^{lo}$ $CD62L^{hi}$ naïve CD8 T cells (1×10^6 per well of a 24-well plate) from CD45.1 C57BL/6 mice were activated in vitro with soluble anti-CD3 (0.1 μg/ml; 145-2C11) and anti-CD28 (1 μg/ml; 37.51) antibodies in plates coated with goat anti-hamster immunoglobulin G (18 μg/ml; Jackson ImmunoResearch, #127-005-099) in the presence of 1×10^3 IU human interleukin-2 (hIL-2). Twenty seven hours after stimulation, cells were spinfected (37°C at 1300*g* for 2 hours) with the indicated pMHCII-CAR RVs (1 ml of viral supernatant per each well) and subsequently cultured with hIL-2 (1×10^3 IU/ml; Teceleukin, Hoffmann-La Roche) before use. Cells cultured for two additional days were used for depletion assays of target TCR Tg cells in vivo. Longer cultures for four to six additional days were conducted for EAE experiments. CAR T cell transfer was performed

in mice without preconditioning by lymphodepletion or irradiation.

Depletion of TCR Tg target T cells in vivo

Congenically marked LN cells from TCR Tg mice (target TCR Tg T cells; 2×10^5) were transferred retro-orbitally into hosts followed 1 day later by transfer of 2×10^5 pMHCII-CAR T cells. After 5 to 7 more days, the frequency of remaining TCR Tg cells in the MLNs was assessed by flow cytometry. For normalizing 2D2 target survival in depletion experiments with MOG-pMHCII CAR T cells, equal numbers (2×10^5) of OTII cells were transferred.

EAE induction and clinical score assessment

Active EAE was induced as previously described (*49*). Briefly, mice were subcutaneously injected with 200 μg of $MOG_{35–55}$ peptide emulsified in FCA and intraperitoneally injected with 200 ng of PTX. After 48 hours, mice received a second dose of PTX. To assess potential side effect of CAR T treatment, we treated mice with 100 μg of $MOG_{35–55}$ peptide and 300 ng of PTX in Fig. 5 (G and H) for a less severe clinical phenotype (*32*). Mice were observed daily, and clinical score was assessed with a five-point scoring system: 0, no disease; 1, limp tail; 2, mild hind limb paresis; 3, severe hind limb paresis; 4, complete hind limb plegia or quadriplegia; and 5, moribund or dead.

CNS cell preparation for flow cytometric analysis

CNS cell preparation was performed as previously described (*50*). Briefly, mice were perfused with 25 to 30 ml of cold phosphate-buffered saline (PBS) before isolation of CNS tissue. Mononuclear cells were purified separately from homogenized brains and spinal cords by centrifugation for 30 min in 30% percoll (GE Healthcare) solution.

Antibodies and flow cytometry

Isolated cells were washed with PBS containing 1% fetal bovine serum (FBS) and 0.05% sodium azide (VWR) and stained with fluorochrome-conjugated antibodies together with propidium iodide (Life Technologies) to eliminate dead cells. Fluorescently conjugated antibodies (table S3) were purchased from BioLegend, Invitrogen, and Becton Dickinson. For detection of MOG-specific CD4 T cells, CNS cells were stained for 1 hour at room temperature with a mixture of fluorochrome-conjugated antibodies and IA(b)/GWYRSPFSRVVH allophycocyanin (APC)–labeled tetramer [National Institutes of Health (NIH) Tetramer Core Facility] prepared in 10% FBS Dulbecco's modified Eagle's medium. Samples were analyzed using a BD FACSAria IIu (Becton Dickinson), and data were processed with FlowJo 10 (Tree Star).

TCR sequencing and data analysis

T cells were isolated from the PLN (cervical, axillary, brachial, and inguinal LNs) or CNS of TCli TCRβ $Tcra^{+/-}$ $Foxp3^{IRES\text{-}GFP}$ mice. TCR sequencing was performed as previously described (*18*). After TCRα cDNA was synthesized from sorted T cells (*17*), amplification was performed using a multiplex polymerase chain reaction (*18*). MiSeq (250 paired-end reads) sequencing data of T cell populations from individual mice were analyzed via DADA2 (*51*) without bimera filtering to identify amplicon sequence variants and reduce noise due to sequencing errors. TCR sequences were parsed as before to identify the TRAV and CDR3 amino acid sequences, which together are used to designate a unique TCR (*18*). TCR repertoires were analyzed in R using Phyloseq, DESeq2, and Vegan (table S4). Candidate $MOG_{35–55}$-specific TCRs were selected and gene-synthesized for further investigations. High-frequency candidate TCRs both from in vitro expansion and PLN/CNS of immunized mice were selected. Low-frequency candidate TCRs were identified by differentially induced TCR analysis using DESeq2. Estimated EC_{50} values calculated by in vitro NFAT-GFP hybridoma assays with RV transduced TCRs were used to correlate affinities and frequencies in the TCR repertoire analysis.

Statistical analysis

Mean and SEM values were calculated by using Prism 9 (GraphPad; table S4). Statistical significance was typically determined by unpaired Student's *t* test or by one-way ANOVA, followed by Holm-Sidak multiple comparison testing. For comparing TCR frequencies, which are not normally distributed, Kruskal-Wallis testing was performed. In vitro assays were analyzed by nested Student's *t* test or nested one-way ANOVA. Repeated measures ANOVA was used for EAE scores over time as indicated. The number of biological replicates, independent experiments (expt.), and statistical tests are indicated in figure legends. *P* values less than 0.05 were considered significant.

Supplementary Materials

This PDF file includes:
Figs. S1 to S7
Tables S1 to S4
Reference (*52*)

Other Supplementary Material for this manuscript includes the following:
Data file S1

View/request a protocol for this paper from *Bio-protocol*.

REFERENCES AND NOTES

1. S. S. Zamvil, D. J. Mitchell, A. C. Moore, K. Kitamura, L. Steinman, J. B. Rothbard, T-cell epitope of the autoantigen myelin basic protein that induces encephalomyelitis. *Nature* **324**, 258–260 (1986).
2. M. Varrin-Doyer, A. Shetty, C. M. Spencer, U. Schulze-Topphoff, M. S. Weber, C. C. Bernard, T. Forsthuber, B. A. Cree, A. J. Slavin, S. S. Zamvil, MOG transmembrane and cytoplasmic domains contain highly stimulatory T-cell epitopes in MS. *Neurol. Neuroimmunol. Neuroinflamm.* **1**, e20 (2014).
3. E. M. Hur, S. Youssef, M. E. Haws, S. Y. Zhang, R. A. Sobel, L. Steinman, Osteopontin-induced relapse and progression of autoimmune brain disease through enhanced survival of activated T cells. *Nat. Immunol.* **8**, 74–83 (2007).
4. P. A. Savage, J. J. Boniface, M. M. Davis, A kinetic basis for T cell receptor repertoire selection during an immune response. *Immunity* **10**, 485–492 (1999).
5. D. A. Price, J. M. Brenchley, L. E. Ruff, M. R. Betts, B. J. Hill, M. Roederer, R. A. Koup, S. A. Migueles, E. Gostick, L. Wooldridge, A. K. Sewell, M. Connors, D. C. Douek, Avidity for antigen shapes clonal dominance in $CD8^+$ T cell populations specific for persistent DNA viruses. *J. Exp. Med.* **202**, 1349–1361 (2005).
6. J. J. Sabatino Jr., J. Shires, J. D. Altman, M. L. Ford, B. D. Evavold, Loss of IFN-γ enables the expansion of autoreactive $CD4^+$ T cells to induce experimental autoimmune encephalomyelitis by a nonencephalitogenic myelin variant antigen. *J. Immunol.* **180**, 4451–4457 (2008).
7. R. W. Nelson, D. Beisang, N. J. Tubo, T. Dileepan, D. L. Wiesner, K. Nielsen, M. Wuthrich, B. S. Klein, D. I. Kotov, J. A. Spanier, B. T. Fife, J. J. Moon, M. K. Jenkins, T cell receptor cross-reactivity between similar foreign and self peptides influences naive cell population size and autoimmunity. *Immunity* **42**, 95–107 (2015).

8. J. J. Sabatino Jr., J. Huang, C. Zhu, B. D. Evavold, High prevalence of low affinity peptide-MHC II tetramer-negative effectors during polyclonal CD4$^+$ T cell responses. *J. Exp. Med.* **208**, 81–90 (2011).
9. K. M. Rosenthal, L. J. Edwards, J. J. Sabatino Jr., J. D. Hood, H. A. Wasserman, C. Zhu, B. D. Evavold, Low 2-dimensional CD4 T cell receptor affinity for myelin sets in motion delayed response kinetics. *PLOS ONE* **7**, e32562 (2012).
10. A. V. Joglekar, M. T. Leonard, J. D. Jeppson, M. Swift, G. Li, S. Wong, S. Peng, J. M. Zaretsky, J. R. Heath, A. Ribas, M. T. Bethune, D. Baltimore, T cell antigen discovery via signaling and antigen presenting bifunctional receptors. *Nat. Methods* **16**, 191–198 (2019).
11. S. E. Starwalt, E. L. Masteller, J. A. Bluestone, D. M. Kranz, Directed evolution of a single-chain class II MHC product by yeast display. *Protein Eng.* **16**, 147–156 (2003).
12. S. K. Lathrop, S. M. Bloom, S. M. Rao, K. Nutsch, C. W. Lio, N. Santacruz, D. A. Peterson, T. S. Stappenbeck, C.-S. Hsieh, Peripheral education of the immune system by colonic commensal microbiota. *Nature* **478**, 250–254 (2011).
13. S. L. Cunliffe, J. R. Wyer, J. K. Sutton, M. Lucas, G. Harcourt, P. Klenerman, A. J. McMichael, A. D. Kelleher, Optimization of peptide linker length in production of MHC class II/peptide tetrameric complexes increases yield and stability, and allows identification of antigen-specific CD4$^+$T cells in peripheral blood mononuclear cells. *Eur. J. Immunol.* **32**, 3366–3375 (2002).
14. S. Jutz, J. Leitner, K. Schmetterer, I. Doel-Perez, O. Majdic, K. Grabmeier-Pfistershammer, W. Paster, J. B. Huppa, P. Steinberger, Assessment of costimulation and coinhibition in a triple parameter T cell reporter line: Simultaneous measurement of NF-κB, NFAT and AP-1. *J. Immunol. Methods* **430**, 10–20 (2016).
15. L. Poncette, X. Chen, F. K. Lorenz, T. Blankenstein, Effective NY-ESO-1-specific MHC II-restricted T cell receptors from antigen-negative hosts enhance tumor regression. *J. Clin. Invest.* **129**, 324–335 (2019).
16. H.-M. Lee, J. L. Bautista, J. Scott-Browne, J. F. Mohan, C.-S. Hsieh, A broad range of self-reactivity drives thymic regulatory T cell selection to limit responses to self. *Immunity* **37**, 475–486 (2012).
17. J. N. Chai, Y. Peng, S. Rengarajan, B. D. Solomon, T. L. Ai, Z. Shen, J. S. A. Perry, K. A. Knoop, T. Tanoue, S. Narushima, K. Honda, C. O. Elson, R. D. Newberry, T. S. Stappenbeck, A. L. Kau, D. A. Peterson, J. G. Fox, C. S. Hsieh, *Helicobacter* species are potent drivers of colonic T cell responses in homeostasis and inflammation. *Sci. Immunol.* **2**, eaal5068 (2017).
18. E. V. Russler-Germain, J. Jung, A. T. Miller, S. Young, J. Yi, A. Wehmeier, L. E. Fox, K. J. Monte, J. N. Chai, D. H. Kulkarni, L. J. Funkhouser-Jones, G. Wilke, V. Durai, B. H. Zinselmeyer, R. S. Czepielewski, S. Greco, K. M. Murphy, R. D. Newberry, L. D. Sibley, C.-S. Hsieh, Commensal *Cryptosporidium* colonization elicits a cDC1-dependent Th1 response that promotes intestinal homeostasis and limits other infections. *Immunity* **54**, 2547–2564.e7 (2021).
19. S. Koehli, D. Naeher, V. Galati-Fournier, D. Zehn, E. Palmer, Optimal T-cell receptor affinity for inducing autoimmunity. *Proc. Natl. Acad. Sci. U.S.A.* **111**, 17248–17253 (2014).
20. D. Zehn, M. J. Bevan, T cells with low avidity for a tissue-restricted antigen routinely evade central and peripheral tolerance and cause autoimmunity. *Immunity* **25**, 261–270 (2006).
21. P. Sinai, I. M. Dozmorov, R. Song, P. L. Schwartzberg, E. K. Wakeland, C. Wülfing, T/B-cell interactions are more transient in response to weak stimuli in SLE-prone mice. *Eur. J. Immunol.* **44**, 3522–3531 (2014).
22. J. M. Robertson, P. E. Jensen, B. D. Evavold, DO11.10 and OT-II T cells recognize a C-terminal ovalbumin 323–339 epitope. *J. Immunol.* **164**, 4706–4712 (2000).
23. S. Kobayashi, M. A. Thelin, H. L. Parrish, N. R. Deshpande, M. S. Lee, A. Karimzadeh, M. A. Niewczas, T. Serwold, M. S. Kuhns, A biomimetic five-module chimeric antigen receptor (^{5M}CAR) designed to target and eliminate antigen-specific T cells. *Proc. Natl. Acad. Sci. U.S.A.* **117**, 28950–28959 (2020).
24. E. Bettelli, M. Pagany, H. L. Weiner, C. Linington, R. A. Sobel, V. K. Kuchroo, Myelin oligodendrocyte glycoprotein-specific T cell receptor transgenic mice develop spontaneous autoimmune optic neuritis. *J. Exp. Med.* **197**, 1073–1081 (2003).
25. A. Jäger, V. Dardalhon, R. A. Sobel, E. Bettelli, V. K. Kuchroo, Th1, Th17, and Th9 effector cells induce experimental autoimmune encephalomyelitis with different pathological phenotypes. *J. Immunol.* **183**, 7169–7177 (2009).
26. B. D. Stadinski, L. Zhang, F. Crawford, P. Marrack, G. S. Eisenbarth, J. W. Kappler, Diabetogenic T cells recognize insulin bound to IAg7 in an unexpected, weakly binding register. *Proc. Natl. Acad. Sci. U.S.A.* **107**, 10978–10983 (2010).
27. H. Karlsson, A. C. Lindqvist, M. Fransson, G. Paul-Wetterberg, B. Nilsson, M. Essand, K. Nilsson, P. Frisk, H. Jernberg-Wiklund, A. Loskog, Combining CAR T cells and the Bcl-2 family apoptosis inhibitor ABT-737 for treating B-cell malignancy. *Cancer Gene Ther.* **20**, 386–393 (2013).
28. T. N. Yamamoto, P. H. Lee, S. K. Vodnala, D. Gurusamy, R. J. Kishton, Z. Yu, A. Eidizadeh, R. Eil, J. Fioravanti, L. Gattinoni, J. N. Kochenderfer, T. J. Fry, B. A. Aksoy, J. E. Hammerbacher, A. C. Cruz, R. M. Siegel, N. P. Restifo, C. A. Klebanoff, T cells genetically engineered to overcome death signaling enhance adoptive cancer immunotherapy. *J. Clin. Invest.* **129**, 1551–1565 (2019).
29. L. Riera, M. Gariglio, M. Pagano, O. Gaiola, M. M. Simon, S. Landolfo, Control of murine cytomegalovirus replication in salivary glands during acute infection is independent of the Fas ligand/Fas system. *New Microbiol.* **24**, 231–238 (2001).
30. S. Karray, C. Kress, S. Cuvellier, C. Hue-Beauvais, D. Damotte, C. Babinet, M. Lévi-Strauss, Complete loss of Fas ligand gene causes massive lymphoproliferation and early death, indicating a residual activity of gld allele. *J. Immunol.* **172**, 2118–2125 (2004).
31. J. Gust, R. Ponce, W. C. Liles, G. A. Garden, C. J. Turtle, Cytokines in CAR T cell-associated neurotoxicity. *Front. Immunol.* **11**, 577027 (2020).
32. C.-C. Lin, T. R. Bradstreet, E. A. Schwarzkopf, J. Sim, J. A. Carrero, C. Chou, L. E. Cook, T. Egawa, R. Taneja, T. L. Murphy, J. H. Russell, B. T. Edelson, Bhlhe40 controls cytokine production by T cells and is essential for pathogenicity in autoimmune neuroinflammation. *Nat. Commun.* **5**, 3551 (2014).
33. P. Wong, A. W. Goldrath, A. Y. Rudensky, Competition for specific intrathymic ligands limits positive selection in a TCR transgenic model of CD4$^+$ T cell development. *J. Immunol.* **164**, 6252–6259 (2000).
34. E. Kieback, E. Hilgenberg, U. Stervbo, V. Lampropoulou, P. Shen, M. Bunse, Y. Jaimes, P. Boudinot, A. Radbruch, U. Klemm, A. A. Kühl, R. Liblau, N. Hoevelmeyer, S. M. Anderton, W. Uckert, S. Fillatreau, Thymus-derived regulatory T cells are positively selected on natural self-antigen through cognate interactions of high functional avidity. *Immunity* **44**, 1114–1126 (2016).
35. K. B. Whittington, A. Prislovsky, J. Beaty, L. Albritton, M. Radic, E. F. Rosloniec, CD8$^+$ T cells expressing an HLA-DR1 chimeric antigen receptor target autoimmune CD4$^+$ T cells in an antigen-specific manner and inhibit the development of autoimmune arthritis. *J. Immunol.* **208**, 16–26 (2022).
36. B. Akkaya, Y. Oya, M. Akkaya, J. Al Souz, A. H. Holstein, O. Kamenyeva, J. Kabat, R. Matsumura, D. W. Dorward, D. D. Glass, E. M. Shevach, Regulatory T cells mediate specific suppression by depleting peptide-MHC class II from dendritic cells. *Nat. Immunol.* **20**, 218–231 (2019).
37. D. E. J. Klawon, D. C. Gilmore, J. D. Leonard, C. H. Miller, J. L. Chao, M. T. Walker, R. K. Duncombe, K. S. Tung, E. J. Adams, P. A. Savage, Altered selection on a single self-ligand promotes susceptibility to organ-specific T cell infiltration. *J. Exp. Med.* **218**, e20200701 (2021).
38. K. Schober, F. Voit, S. Grassmann, T. R. Muller, J. Eggert, S. Jarosch, B. Weißbrich, P. Hoffmann, L. Borkner, E. Nio, L. Fanchi, C. R. Clouser, A. Radhakrishnan, L. Mihatsch, P. Lückemeier, J. Leube, G. Dössinger, L. Klein, M. Neuenhahn, J. D. Oduro, L. Cicin-Sain, V. R. Buchholz, D. H. Busch, Reverse TCR repertoire evolution toward dominant low-affinity clones during chronic CMV infection. *Nat. Immunol.* **21**, 434–441 (2020).
39. R. J. Martinez, R. Andargachew, H. A. Martinez, B. D. Evavold, Low-affinity CD4$^+$ T cells are major responders in the primary immune response. *Nat. Commun.* **7**, 13848 (2016).
40. P. van den Elzen, J. S. Menezes, A. Ametani, E. Maverakis, L. Madakamutil, X.-L. Tang, V. Kumar, E. E. Sercarz, Limited clonality in autoimmunity: Drivers and regulators. *Autoimmun. Rev.* **3**, 524–529 (2004).
41. W. Fu, G. Wojtkiewicz, R. Weissleder, C. Benoist, D. Mathis, Early window of diabetes determinism in NOD mice, dependent on the complement receptor CRIg, identified by noninvasive imaging. *Nat. Immunol.* **13**, 361–368 (2012).
42. S. E. Regnell, Å. Lernmark, Early prediction of autoimmune (type 1) diabetes. *Diabetologia* **60**, 1370–1381 (2017).
43. D. Leslie, P. Lipsky, A. L. Notkins, Autoantibodies as predictors of disease. *J. Clin. Invest.* **108**, 1417–1422 (2001).
44. M. R. Arbuckle, M. T. McClain, M. V. Rubertone, R. H. Scofield, G. J. Dennis, J. A. James, J. B. Harley, Development of autoantibodies before the clinical onset of systemic lupus erythematosus. *N. Engl. J. Med.* **349**, 1526–1533 (2003).
45. S. Hutfless, P. Matos, M. V. Talor, P. Caturegli, N. R. Rose, Significance of prediagnostic thyroid antibodies in women with autoimmune thyroid disease. *J. Clin. Endocrinol. Metab.* **96**, E1466–E1471 (2011).
46. L. Kappos, J. S. Wolinsky, G. Giovannoni, D. L. Arnold, Q. Wang, C. Bernasconi, F. Model, H. Koendgen, M. Manfrini, S. Belachew, S. L. Hauser, Contribution of relapse-independent progression vs relapse-associated worsening to overall confirmed disability accumulation in typical relapsing multiple sclerosis in a pooled analysis of 2 randomized clinical trials. *JAMA Neurol.* **77**, 1132–1140 (2020).
47. H. Wang, P. Han, X. Qi, F. Li, M. Li, L. Fan, H. Zhang, X. Zhang, X. Yang, Bcl-2 enhances chimeric antigen receptor T cell persistence by reducing activation-induced apoptosis. *Cancers (Basel)* **13**, 197 (2021).
48. W. S. Pear, G. P. Nolan, M. L. Scott, D. Baltimore, Production of high-titer helper-free retroviruses by transient transfection. *Proc. Natl. Acad. Sci. U.S.A.* **90**, 8392–8396 (1993).

49. G. F. Wu, K. S. Shindler, E. J. Allenspach, T. L. Stephen, H. L. Thomas, R. J. Mikesell, A. H. Cross, T. M. Laufer, Limited sufficiency of antigen presentation by dendritic cells in models of central nervous system autoimmunity. *J. Autoimmun.* **36**, 56–64 (2011).
50. C. R. Parker Harp, A. S. Archambault, M. Cheung, J. W. Williams, R. S. Czepielewski, P. C. Duncker, A. J. Kilgore, A. T. Miller, B. M. Segal, A. H. J. Kim, G. J. Randolph, G. F. Wu, Neutrophils promote VLA-4-dependent B cell antigen presentation and accumulation within the meninges during neuroinflammation. *Proc. Natl. Acad. Sci. U.S.A.* **116**, 24221–24230 (2019).
51. B. J. Callahan, P. J. McMurdie, M. J. Rosen, A. W. Han, A. J. Johnson, S. P. Holmes, DADA2: High-resolution sample inference from Illumina amplicon data. *Nat. Methods* **13**, 581–583 (2016).
52. Y. L. Cho, M. Flossdorf, L. Kretschmer, T. Hofer, D. H. Busch, V. R. Buchholz, TCR signal quality modulates fate decisions of single $CD4^+$ T cells in a probabilistic manner. *Cell Rep.* **20**, 806–818 (2017).

Acknowledgments: The following reagent was obtained through the NIH Tetramer Core Facility: IA(b)/GWYRSPFSRVVH APC-labeled tetramer. We thank T. Bigley and M. Paley (Washington University in St. Louis) for critical reading of the manuscript. **Funding:** This study was supported by R01-AI07987 and the Wolff Professorship (to C.-S.H), NINDS (R01NS106289) and the National Multiple Sclerosis Society (RG-1802-30253) (to G.F.W.), NIAID (R01AI165771) (C.S.H. and G.F.W.), NCI (K08CA237740) (to N.S.), and the National Multiple Sclerosis Society (RG-2111-38724) (to B.T.E.). **Author contributions:** J.Y., A.T.M., G.F.W., and C.-S.H. conceived the project and/or designed the experiments. J.Y., A.T.M., A.S.A., A.J.J., T.R.B., Y.-S.H., N.S., and S.B. performed the experiments. J.Y. did TCR repertoire analysis. C.-S.H., Y.W.Z., D.H.F., N.S., and T.E. discussed CAR engineering. G.F.W., B.T.E., and C.-S.H. discussed the EAE model. J.Y., A.T.M., G.F.W., and C.-S.H. wrote the manuscript. **Competing interests:** The authors declare that they have no competing interests. **Data and materials availability:** All data needed to evaluate the conclusions in the paper are present in the paper or the Supplementary Materials. TCR sequencing data have been deposited at the European Nucleotide Archive (ENA) and are publicly available under accession number PRJEB53445. pMHCII-CAR and TCR expression plasmids are available upon request via material transfer agreement with Washington University in St. Louis.

Submitted 12 January 2022
Accepted 15 September 2022
Published 7 October 2022
10.1126/sciimmunol.abo0777